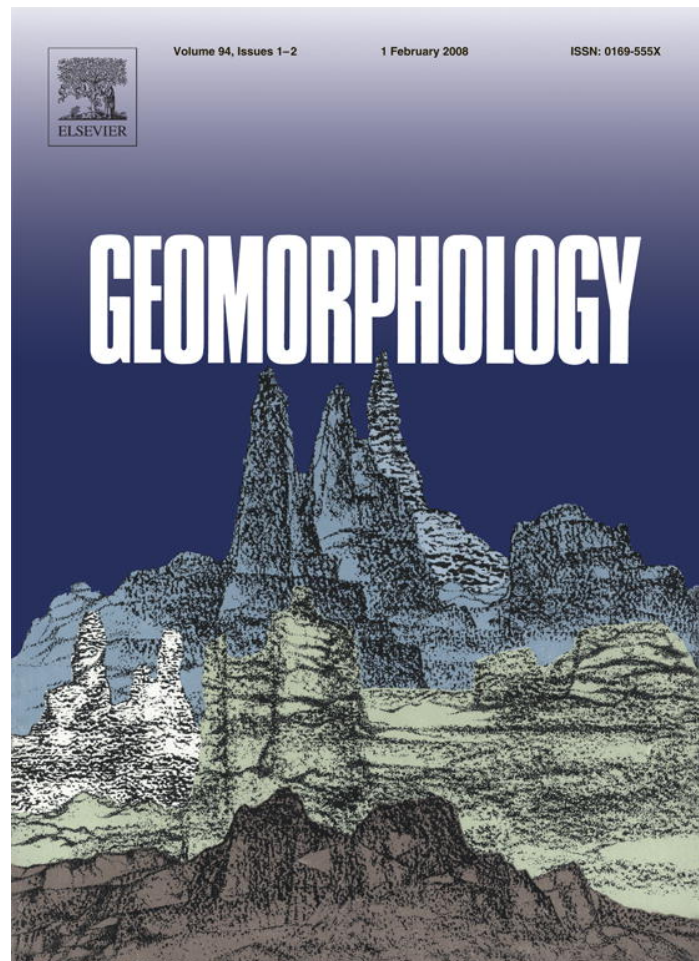


Provided for non-commercial research and education use.
Not for reproduction, distribution or commercial use.



This article was published in an Elsevier journal. The attached copy is furnished to the author for non-commercial research and education use, including for instruction at the author's institution, sharing with colleagues and providing to institution administration.

Other uses, including reproduction and distribution, or selling or licensing copies, or posting to personal, institutional or third party websites are prohibited.

In most cases authors are permitted to post their version of the article (e.g. in Word or Tex form) to their personal website or institutional repository. Authors requiring further information regarding Elsevier's archiving and manuscript policies are encouraged to visit:

<http://www.elsevier.com/copyright>



A probabilistic model of debris-flow delivery to stream channels, demonstrated for the Coast Range of Oregon, USA

Daniel J. Miller^{a,*}, Kelly M. Burnett^b

^a *Earth Systems Institute, 3040 NW 57th Street, Seattle, WA 98107, USA*

^b *Pacific Northwest Research Station, USDA Forest Service, Corvallis, Oregon, 97331, USA*

Received 30 November 2006; received in revised form 9 May 2007; accepted 12 May 2007

Available online 2 June 2007

Abstract

Debris flows are important geomorphic agents in mountainous terrains that shape channel environments and add a dynamic element to sediment supply and channel disturbance. Identification of channels susceptible to debris-flow inputs of sediment and organic debris, and quantification of the likelihood and magnitude of those inputs, are key tasks for characterizing spatial and temporal patterns found in channel conditions and associated habitats in a river network. Widely available digital elevation and land-cover data (10-m DEMs and 25-m satellite imagery) offer the potential to assess debris-flow runout paths over regional extents. This paper presents a model for using these data to calculate empirical probabilities for debris-flow runout over DEM-determined flow paths and shows how these probabilities can be combined over all sources to estimate the potential for debris-flow delivery to stream reaches throughout entire channel networks. The model is calibrated and model predictions are compared to field-mapped debris-flow travel paths from study sites in the Coast Range of Oregon, USA. This model predicts debris-flow probability over channel-reach scales that can be aggregated to basin-scale measures of debris-flow potential. It offers unprecedented ability to characterize debris-flow effects over channel networks, providing a tool for risk assessment and for generating hypotheses that relate topographic and forest-cover controls on debris-flow runout to the types and abundance of channel habitats in a river basin.

© 2007 Elsevier B.V. All rights reserved.

Keywords: Debris flow; Landslide; Disturbance; Aquatic habitat; Risk assessment

1. Introduction

Landslides and debris flows are important geomorphic agents in mountainous terrain and can greatly affect mountain stream ecosystems (Swanson et al., 1988, 1998). Debris fans and terraces constrain channel planform and cross-sectional geometry; boulders and wood in debris-flow deposits form persistent sources of

channel roughness (Benda, 1990; Wohl and Pearthree, 1991; Brummer and Montgomery, 2003). Debris-flow depositional sites, thereby, contribute to aquatic habitat heterogeneity (Benda et al., 2003; Bigelow et al., 2007). Debris flows are also important sources of channel disturbance, scouring centuries of accumulated sediment and organic debris from headwater streams, and inundating valley floors in their deposits (Hack and Goodlett, 1960; Cenderelli and Kite, 1998; Miller and Benda, 2000; May and Gresswell, 2003). Characterization of debris-flow locations and rates of occurrence are

* Corresponding author. Tel.: +1 206 633 1792.

E-mail address: danmiller@earthsystems.net (D.J. Miller).

thus key factors in analysis of mountain river geomorphology and associated ecosystems (Benda et al., 2004; May and Gresswell, 2004). The role of debris flows in driving ecosystem dynamics is of particular concern in areas managed for timber production, because evidence points to timber harvest and road construction as prominent controls on where and how often landslides and associated debris flows occur (Swanson and Dyrness, 1975; Montgomery et al., 2000).

Our goal was to develop methods for identifying and ranking stream channels subject to landslide-triggered debris-flows over areas spanning 10^1 to 10^4 km². Analysis over these spatial extents constrained us to using available digital data with geographical information system (GIS) software. We approached this task in two phases. In the first, we characterized susceptibility of hillslopes to debris-flow triggering landslides (Miller and Burnett, 2007). In the second, described here, we characterized potentials for debris-flow runout from identified landslide source areas. Both phases relied on the same strategy: 1) identify the pertinent processes and specify a priori topographic and forest-cover attributes that influence landslide susceptibility and debris-flow runout, based on observations and measurements reported in previous studies, 2) define spatially distributed, digital characterizations (maps) of these attributes, 3) overlay mapped landslides and debris-flow tracks on these digital maps, and 4) define empirical probabilities of encountering a mapped landslide or debris-flow track in terms of the specified attributes. We characterized landslide susceptibility in terms of topographic attributes derived from 10-m-grid digital elevation models (DEMs), forest-cover classes based on classified satellite imagery, and vicinity to mapped forest roads (Miller and Burnett, 2007). Our objective now is to characterize debris-flow tracks in terms of forest-cover class and DEM-inferred gradient, flow-path confinement, and channel-network geometry to provide an empirical probability that a debris flow continued from its originating location downslope cell-to-cell along a DEM-delineated flow path. We describe methods to estimate runout probabilities for a single debris flow and to incorporate multiple debris-flow sources to calculate a relative probability that a channel reach contains a mapped debris-flow track.

Two basic approaches have been used for empirical models of debris-flow runout: those using the ratio of total vertical and horizontal displacement of the debris-flow mass (Bathurst et al., 1997; Iverson, 1997; Rickenmann, 1999) and those using local measures of runout path geometry (Benda and Cundy, 1990; Cannon 1993; Iverson et al., 1998; Fannin and Wise, 2001). We have

taken the second approach, which can accommodate changes in debris-flow volume associated with scour and deposition along the runout path, and which also benefits from the topographic detail available in current DEMs. Several variations of this approach have been implemented in GIS-based models (Ellen and Mark, 1993; Schilling, 1998; Hofmeister and Miller, 2003). We build on concepts presented in these earlier studies, focusing particularly on debris-flow delivery to stream channels, on effects of forest cover, and on techniques that can be implemented over regional extents.

2. Methods

2.1. Conceptual basis

Two basic postulates formed the basis of the runout model: 1) the downslope end of a debris-flow deposit, the terminus, indicates the point where the volume entrained equals the volume deposited, and 2) the entrained and deposited volumes can be estimated as functions of attributes along the travel path. We sought to constrain these travel-path attributes over large areas. At these scales, the factors that influence runout length cannot all be resolved, so we took an empirical and probabilistic approach. We used a population of observed debris-flow travel paths to identify the range of attribute values, at the resolution of available data, that characterized locations of mapped debris-flow scour and deposition. From this information, we defined an index of debris-flow volume that varied with travel distance along any potential debris-flow path. We then used the distribution of index values calculated for mapped debris-flow end points to define an empirical probability that a debris flow terminated. This probability is a function of the volume index, which is a function of topographic and forest-cover attributes along the cumulative travel path. From this information, we inferred the likelihood that a debris flow continued downslope from its point of origin to any point along a potential flow path.

Three key observations guided our development of this model:

1. Debris flows entrain material through steep, confined sections of the travel path and deposit material through lower gradient, unconfined sections (Benda and Cundy, 1990; Fannin and Wise, 2001). As a consequence of entrainment along a portion of the runout path, deposited volume correlates with travel length (May, 2002).
2. Debris flows often terminate at channel confluences where the junction angle is large (Benda and Cundy,

1990) and/or where the receiving valley is wide and of low gradient (May, 2002).

3. Debris flows through recently harvested forests tend to travel further, and entrain more material, than those through older stands containing large trees (Robison et al., 1999; May, 2002; Ishikawa et al., 2003; Lancaster et al., 2003).

Although many additional factors affect debris-flow runout, these three observations are particularly pertinent to our goal of quantifying the potential for debris-flow scour and deposition over a channel network. Of crucial importance, the required variables – gradient, topographic confinement, channel junction angles, and forest cover – can all be estimated with available digital data.

2.2. Single debris flow

In the absence of fluvial reworking, the downstream end of a debris-flow deposit indicates the point where volume deposited equals the volume entrained. If volume entrained and volume deposited relate to quantifiable aspects of the travel path (specifically, gradient and channel confinement), then analysis of a potential debris-flow track provides a comparison of scoured to deposited volume and, where the two are equal, gives an estimate of travel distance (Cannon, 1993; Fannin and Wise, 2001). Thus, our analysis of debris-flow runout started by examining observed travel paths.

To differentiate zones of entrainment and deposition, we overlaid on a DEM debris-flow tracks that had been field mapped into sections of scour, transitional flow (no net scour or deposition), and deposition. In an analysis of field observations, Fannin and Rollerson (1993) found that the ratio of channel width to slope gradient delineated zones of scour and deposition. To extend this measure to DEM-derived quantities, from which channel width is not generally resolvable on the 10-m data available, we defined a width-weighted slope (S_W)

$$S_W = \frac{\sin \theta}{w} \quad (1)$$

where θ is surface gradient, estimated from the DEM using a nine-point surface polynomial as described by Zevenbergen and Thorne (1987), and w is a measure of confining width defined using measures of surface geometry obtained directly from the DEM:

$$w = 1 - \arctan \left(1 - \frac{W_V}{W_{V1}} \right). \quad (2)$$

Here W_V is valley width and W_{V1} is a normalizing constant set to the mean width of first-order valleys (see Table 1 for a complete list of symbols). We did not use W_V directly in Eq. (1), because (as explained below) our algorithm for measuring W_V in some cases greatly over estimated valley width. The use of an asymptotic function minimized the influence of these errors. The function w is less than one when W_V is less than W_{V1} , and increases asymptotically to a limiting value of 2.57 (one minus the arctangent of minus infinity) as W_V increases indefinitely. Along delineated channels, W_V was estimated as the shortest transect intersecting opposite valley walls at a height of some multiple of

Table 1
List of symbols

S_W	Width-weighted slope, Eq. (1)
θ	Ground-surface gradient, Eq. (1)
w	Measure of confining width, Eq. (2)
W_V	Valley width, Eq. (2)
P_S	Probability of debris-flow scour, Eqs. (3) and (6)
P_T	Probability of debris-flow transitional flow, Eqs. (4) and (8)
P_{Dep}	Probability of debris-flow deposition, Eqs. (5) and (7)
V_S	Index proportional to volume entrained by debris flow along the travel path, Eq. (11)
V_D	Index proportional to volume deposited by debris flow along the travel path, Eq. (12)
L	Debris flow travel distance, Eq. (14)
F	Cumulative distribution of a population of debris-flow travel distances, Eqs. (14) and (18)
R	Natural logarithm of the ratio of volume deposited to volume entrained, Eq. (15)
p_R	Adjustment to probability that a debris flow terminated in a travel increment, Eq. (16)
F_R	Cumulative distribution of debris-flow endpoint R values, Eq. (16)
L_R	Weighted debris-flow travel length, Eq. (17)
P_R	Probability that a debris flow reached a point downslope of its origin, Eq. (19)
V_{DF}	Index of debris-flow volume, Eq. (20)
θ_j	Tributary junction angle
p_j	Probability that a debris flow continued through a channel junction
P_j	Probability that a debris flow traveled through all upstream channel junctions, Eq. (21)
p_{DEL}	Probability that a debris flow occurred from a specific point and traveled to a specific point downslope, Eq. (22)
P_{LS}	Probability of a mapped debris-flow triggering landslide, Eq. (22)
P_{DEL}	Probability that a debris flow from any upslope point occurred and traveled to a specified point, Eq. (24)
L_C	Cumulative travel length of debris flows over a specified area, Eq. (25)
V_R	Debris-flow-deposit volume remaining in the receiving channel, with the rest removed by fluvial erosion, Eq. (26)
SA	The slope (m/m)–area (km ²) product, Eq. (26); an index of total stream power

bank-full depth above the channel. Bank-full depth can be estimated from a regional regression of measured bank-full depths to drainage area. With the 10-m DEMs, placement of the cross-valley transect at a height of five bank-full depths above the channel gave the best correspondence to estimates of valley width made from 1:24,000-scale topographic maps. However, in some cases, particularly for small, low-gradient channels, the cross-valley transect missed the adjacent valley walls, leading to an undefined or unrealistically wide estimate of W_v . When this happened, the use of Eq. (2) limited estimates of confinement w to the maximum value of 2.57. For unchannelized hillslope swales, W_v was estimated at a height of 2 m using cross-slope curvature from the nine-node surface polynomial. This height gave valley widths for first-order channels similar to those obtained with the cross-valley transect. Large values of S_w correspond to steep, confined channels and gullies; small values correspond to less-steep, unconfined channels and swales.

DEM cells intersected by debris-flow tracks were separated according to field-identified type (scour, transitional flow, or deposition) and ranked by increasing S_w value. Over any small increment, ΔS_w , the proportion in each type defines an empirical probability that a cell was mapped in a zone of scour (P_S), transitional flow (P_T), or deposition (P_{Dep}):

$$P_S(S_w) = \frac{\Delta n_S(S_w)}{n(S_w)} \quad (3)$$

$$P_T(S_w) = \frac{\Delta n_T(S_w)}{n(S_w)} \quad (4)$$

$$P_{Dep}(S_w) = \frac{\Delta n_{Dep}(S_w)}{n(S_w)}. \quad (5)$$

Here $\Delta n_S(S_w)$, $\Delta n_T(S_w)$, and $\Delta n_{Dep}(S_w)$ are the number of cells mapped as scour, transitional, or depositional, respectively, over the range $S_w \pm \Delta S_w$, and $n(S_w)$ is the total number of cells in the increment: $n(S_w) = \Delta n_S(S_w) + \Delta n_T(S_w) + \Delta n_{Dep}(S_w)$. Out of all DEM cells traversed by mapped debris-flow-tracks, Eqs. (3)–(5) indicate the proportion of cells within the range $S_w \pm \Delta S_w$ that are in each type. P_S , P_T , and P_{Dep} vary over the full range of S_w values such that, at any point, they sum to unity. High P_S values (i.e., a high proportion of scour cells) are associated with high S_w values and high P_{Dep} values (i.e., a high proportion of deposition cells) are associated with small S_w values.

Values for P_S and P_{Dep} should vary monotonically with S_w . We found that a three-parameter function of the form $(a + bx)^c$ closely matched patterns indicated by field data, giving

$$P_S(S_w) = (a_S + b_S S_w)^{c_S} \quad (6)$$

$$P_{Dep}(S_w) = (a_{Dep} + b_{Dep} S_w)^{c_{Dep}} \quad (7)$$

$$P_T(S_w) = 1 - (P_S + P_{Dep}). \quad (8)$$

Values for coefficients a and b are constrained by the S_w values at which the proportions specified in Eqs. (3) and (5) become zero (S_{w0}) and one (S_{w1}):

$$a = \frac{S_{w1}}{S_{w0} - S_{w1}} \quad (9)$$

$$b = \frac{1}{S_{w1} - S_{w0}} \quad (10)$$

The S_{w0} value for P_S was set to the smallest observed S_w value associated with scour, leaving five free coefficients (S_{w1} for scour, S_{w0} and S_{w1} for deposition, c_S , and c_{Dep}) to determine for Eqs. (6) and (7), with the further constraint that $P_S + P_{Dep} \leq 1$. Coefficient values were set using a least-squares fit to the cumulative channel lengths, plotted against S_w , for field-mapped zones of scour, transitional flow, and deposition. For S_w values smaller than S_{w0} for scour, P_S was set to zero; for values greater than S_{w1} for scour, P_S was set to one. Likewise, for S_w values smaller than S_{w1} for deposition, P_{Dep} was set to one; for values greater than S_{w0} for deposition, P_{Dep} was set to zero. To assess the influence of forest cover, this calibration was determined separately for different cover types. The empirical probabilities defined in Eqs. (6) and (7) differentiate zones of potential scour and deposition over all channels.

For a potential debris-flow track, we assumed that the volume entrained is proportional to the length of the scour zone; i.e., the volume entrained is the unknown entrainment rate ($m^3 m^{-1}$) multiplied by the scour-zone length. The scour-zone length was estimated by integrating the probability of scour along the debris-flow track, or in the digital case, summing over cells:

$$\text{Volume entrained} \propto V_S = \sum P_{Si} l_i. \quad (11)$$

Here P_{Si} is the probability of scour of the i -th cell along the runout track, l_i is the length of the runout track through the i -th cell, and V_S is a measure proportional to the potential cumulative scoured (entrained) volume.

Likewise, we assumed that the volume deposited is proportional to the length of the depositional zone, with two additional factors: the volume deposited per unit length of travel was assumed to increase with total volume and with valley width. Larger debris flows leave deeper deposits, and broader valleys have wider deposits. Iverson et al. (1998) suggested that the planimetric area of debris-flow deposits is proportional to volume deposited to the two-thirds power, or that mean depth of deposition is proportional to volume to the one-third power. Although focused on debris-flow deposits created by volcanic lahars, Iverson et al. (1998) also presented data on smaller, non-volcanic debris flows in their Fig. 6. With these assumptions, we defined V_D , a measure proportional to the potential cumulative volume deposited as

$$\text{Volume Deposited} \propto V_D = \sum V_{Si}^{1/3} P_{\text{Dep}i} l_i w_i \quad (12)$$

where V_{Si} is proportional to the cumulative volume entrained, Eq. (6), at the i -th cell; $P_{\text{Dep}i}$ is the probability of deposition, Eq. (7), l_i is the length, and w_i is the measure of confining width defined in Eq. (2), all for the i -th cell.

The debris-flow deposit extends to where the volume scoured equals the volume deposited. Both V_S and V_D were defined as proportional to these volumes, so at the endpoint of the deposit we had

$$\frac{a_D V_D}{V_S} = 1. \quad (13)$$

Here a_D is a constant of proportionality between Eqs. (11) and (12), which we estimated from calculated values of V_S and V_D at the endpoints of field-mapped runout tracks ($a_D = V_S / V_D$) using the scour and depositional probabilities along the tracks defined by Eqs. (6) and (7). In fact, the value of a_D calculated from Eq. (13) varies with every debris flow, reflecting variability in the factors that affect actual debris-flow volumes. These factors include, for example, the volume of the initiating landslide and the volume available for entrainment per unit length of scour (Benda, 1990; May, 2002), which depend on details of topography and geology, on rates of soil production and transport (Dietrich and Dunne, 1978), and on time since the last debris flow (May and Gresswell, 2003). Perhaps such factors can be determined for a site-specific analysis, but we cannot constrain them site-by-site, or

cell-by-cell, regionally (Dunne, 1998). Instead, we set a_D to the median value obtained from Eq. (13) for all debris flows in a field survey and then used the observed variability to define an empirical probability for debris-flow runout length.

We started with a basic constraint: the probability that a debris flow reaches any point along a potential flow path must not increase with increasing travel distance. The probability of reaching a point downstream cannot increase because the debris flow must traverse all intermediate points to get there. In the simplest case, the probability of terminating through any increment ΔL of travel-length L is constant, given by $\lambda \Delta L$, where λ is the probability of terminating per unit travel length. In that case, the probability that a debris flow reaches a downslope point decreases exponentially with distance traveled and the travel lengths from a population of debris flows would follow a cumulative distribution given by:

$$F = \lambda e^{-\lambda L} \quad (14)$$

where L is total travel distance and λ is equal to one over the mean travel distance of all debris flows. This is, in fact, not a bad approximation to measured travel distances when small debris flows are included in the data set (such as those of Lancaster et al., 2003), because there are many short-runout debris flows and few long ones. This simple model, however, treats all debris flows the same; it does not account for attributes of the travel path.

To incorporate the travel path into this model, we defined a quantity R using the left side of Eq. (13):

$$R = \ln \left(\frac{a_D V_D}{V_S} \right). \quad (15)$$

The value of R varies along any potential debris-flow path in response to cumulative travel-path characteristics. Where the upslope portion of the travel path is steep and confined, V_S is large, V_D small, and R is negative. Conversely, where the travel path has extended over low-gradient, unconfined topography, V_D is large and R increases. We used the value of R along a travel path to adjust the probability that a debris flow terminates within the next increment of travel. The adjustment was based on observed debris-flow endpoint R values using the derivative of the empirical cumulative distribution function

$$p_R = \frac{dF_R(R)}{dR} \approx \frac{\Delta n(R)}{N} \quad (16)$$

where $F_R(R)$ is the proportion of observed debris flows with endpoint R values less than or equal to R , $\Delta n(R)$ is the number of values in the increment $R \pm \Delta R$, and N is

the total number of observations. For any point along a potential debris-flow path, the probability that a debris flow terminates in the next increment of travel is now given as $\lambda p_R \Delta L$. Thus, the probability of terminating is decreased where p_R is small; that is, where the cumulative travel path has an R value falling in the range containing a small proportion of observed debris-flow endpoints. Conversely, the probability of terminating is increased where p_R is large; where the cumulative travel path has an R value falling in the range containing a large proportion of observed endpoints. To determine a value for λ , we defined a weighted travel length L_R for every cell along a potential debris-flow travel path:

$$L_R = \sum p_{Ri} l_i. \quad (17)$$

The sum includes all cells along the travel path to the current point, starting with the cell where the debris flow originated. Compared to the actual travel length, $L = \sum l_i$, the weighted length L_R reflects conditions encountered along the way. From Eq. (14), the cumulative distribution of weighted travel lengths is then represented as

$$F = \lambda e^{-\lambda L_R}, \quad (18)$$

and a value for λ is estimated from \bar{L}_R^{-1} , the inverse of the mean weighted travel length determined for a set of field-mapped debris flows. For any potential debris-flow path, the runout probability P_R , i.e., the probability that a debris flow reaches a point downslope, was estimated as

$$P_R = 1 - \lambda e^{-\lambda L_R}. \quad (19)$$

This strategy was derived simply from the observation that debris flows entrain material through steep, confined portions of the travel path and deposit material through low-gradient, unconfined portions.

We next addressed the observation that debris flows often terminate at channel confluences. To characterize channel-junction effects on debris-flow runout, we took an approach similar to that described above: overlay mapped debris-flow tracks on a DEM, extract the pertinent channel-junction attributes, and empirically estimate the probability that a debris flow terminates at the junction based on the proportion of observed debris-flow endpoints associated with specific ranges of attribute values.

We began by determining the pertinent channel-junction attributes to extract. Benda and Cundy (1990), in an analysis of 44 debris flows in the Oregon Coast Range, observed that debris flows would typically continue to channel gradients of about 6% (3.4°), and that debris flows entering confluences where the channels met at high angles often terminated, even

when the receiving channel gradient was greater than 6%. They found that debris flows encountering junction angles exceeding 70° invariably stopped, but suggested that debris flows may continue through very steep channels regardless of the junction angle. These observations were corroborated by Robison et al. (1999) in an analysis of landsliding in western Oregon following a large storm in 1996. Of the 506 surveyed landslides that entered stream channels, 361 were interpreted as debris flows. Of these 361 debris flows, only 8% traveled beyond channel gradients less than 6% or through junction angles exceeding 70°. Robison et al. (1999) note that the 8% of debris flows that traveled further than these gradient and junction-angle thresholds had a mean volume larger than the mean of all debris flows mapped in their study. They also found that those debris flows that stopped at gradients steeper than 6% or that stopped at channel confluences with junction angles less than 70° tended to terminate in mature forests, regardless of the forest type at the initiation point. These observations indicate that junction angle, debris-flow volume, gradient and forest cover of the receiving channel are pertinent attributes to address in the model.

Junction angles (θ_J) were estimated from the planform geometry of the DEM-derived channel network. For each confluence within a network, we defined the channel with the largest drainage area upstream of the confluence as the mainstem and the other channel as the tributary. Orientation of the tributary was estimated using a linear regression through channel DEM points extending 100 m upstream in the tributary from the confluence. Orientation of the mainstem was estimated using a linear regression through DEM channel points extending 100 m upstream and 100 m downstream of the confluence.

An index for debris-flow volume (V_{DF}) was obtained from the difference between V_S , Eq. (11), and V_D , Eq. (12):

$$V_{DF} = V_S - a_D V_D \quad (20)$$

where a_D is the constant of proportionality in Eq. (13). Conceptually, the value of V_{DF} is proportional to the volume entrained minus the volume deposited, and reflects the volume remaining at any point along the debris-flow travel path. V_{DF} varies along the debris-flow path, increasing through zones of scour and decreasing through zones of deposition. Because a_D was set to the median value obtained from Eq. (13), half of all mapped debris-flow endpoints have negative V_{DF} values. Nevertheless, large V_{DF} values indicate portions of the travel path where the volume is potentially large; small

values indicate portions of the travel path where any remaining volume is likely to be small.

Effects of mainstem channel gradient were incorporated in the probability of deposition, P_{Dep} (Eqs. (5) and (7)). P_{Dep} of the mainstem channel also reflects the influence of forest cover, if probabilities for scour, transitional flow, and deposition are calibrated separately for different cover types.

We assembled values for every channel confluence encountered by mapped debris flows traveling from a tributary into a mainstem channel, divided between those through which debris flows continued (“go” junctions) and those at which debris flows terminated (“stop” junctions, indicated by a mapped debris-flow endpoint within 30 m up or downstream of the junction). We considered binning values over increments of each attribute (θ_j , V_{DF} , and P_{Dep}), to create a three-dimensional matrix of bins. The proportion of “go” versus “stop” points within each bin would be an empirical estimate of the probability that a debris flow terminated at a junction, based on the bin it falls into. Unless an extensive data set of field-mapped debris flows is available for populating the bins, the data space is sparsely populated and many bins remain empty.

Instead of binning values, we defined a point density over a three-dimensional grid of points within the data space (θ_j , V_{DF} , and P_{Dep}). The density was calculated by counting points, weighted by distance, over a specified volume centered at each grid point. To provide a continuous estimate of proportions throughout the data space, we used a three-dimensional interpolation technique for finite-element analysis, the 20-node serendipity brick (Zienkiewicz and Taylor, 1988). All internal values are set by the values at 20 nodes on the exterior surface (Fig. 1). Values at the nodes of the brick were set to give the best least-squares fit to the ratio of “go” to total point (sum of the “go” and “stop” points) density at each position within the three-dimensional grid. The probability that a debris flow travels through a channel junction, p_j , was then estimated from the position within the brick determined by the junction angle (θ_j), the volume index of the debris flow at the junction (V_{DF}), and the depositional probability (P_{Dep}) of the receiving channel. The probability of traversing multiple junctions, P_j , was given by the product of each:

$$P_j = \prod p_j \quad (21)$$

where the product is over all upstream junctions.

We could then follow a debris flow from its point of origin and calculate the probability that it reached any downslope point using the product of P_R , the runout

probability given by Eq. (19), and P_j , the probability of traversing all upstream junctions given by Eq. (21). The probability that a debris flow occurred and traveled to a channel (p_{DEL}) is:

$$p_{\text{DEL}} = P_{\text{LS}}P_{\text{R}}P_j \quad (22)$$

where P_{LS} is the probability for a debris-flow triggering landslide, which can be obtained from spatially distributed estimates of landslide density. Landslide probability is an equally important, but separate, aspect of this model, which we treat in detail in a separate paper (Eq. (14) in Miller and Burnett, 2007). Eq. (22), and the steps taken to obtain each of its components, provides a method for estimating the potential for debris-flow transfer of material from any single hillslope location to any point downslope, including any point in the channel network. Eq. (22) incorporates effects of topography and channel geometry along the runout path and can be calibrated to field observations. Importantly for our purposes, it uses representations of topography and channel geometry derived from a DEM (both for calibration and for prediction), so that the model can be implemented in a GIS.

2.3. Multiple debris flows

A point in a channel is potentially subject to debris flows from multiple sources. To assess potential for in-

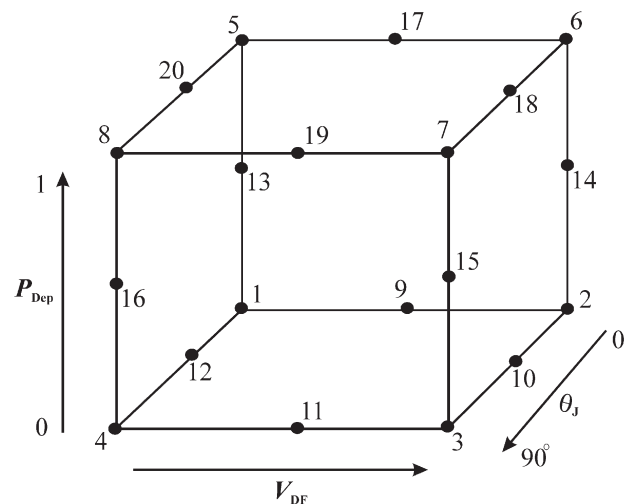


Fig. 1. A 20-node, 3-dimensional serendipity brick for estimating p_j , the probability that a debris flow continues through a tributary junction. Values of depositional probability P_{Dep} in the receiving channel, tributary junction-angle θ_j , and debris-flow-volume index V_{DF} determine position within the brick. Values of p_j are determined at all points within the brick by the values set at the 20 nodes indicated on the surface.

channel effects, we must account for all potential debris flows. We can use the product of probability over all potential sources, but the product of p_{DEL} over all sources would give the vanishingly small probability that every one of them failed and delivered material to the stream. To calculate the probability that any single source, out of all potential sources, failed and delivered, we must use the probability of no delivery from any source. The probability of no delivery from a single source is given simply by $1 - p_{DEL}$, from which we obtained the probability of no delivery from any source (P_{NO_DEL}), and subsequently, the probability for delivery from any source (P_{DEL}):

$$P_{NO_DEL} = \prod(1 - p_{DEL})_i \quad (23)$$

$$P_{DEL} = 1 - P_{NO_DEL} \quad (24)$$

To implement Eq. (23), we created a P_{NO_DEL} grid with a starting value of one for every cell. We then marched through the DEM, cell by cell, and for all cells

with a landslide initiation probability, P_{LS} , greater than zero, we traced the downslope travel path. For each cell encountered along the travel path, we calculate the no-delivery probability, $1 - p_{DEL}$, multiplied the corresponding cell in the P_{NO_DEL} grid by this value, and then updated the P_{NO_DEL} grid. We continued along the flow path until the no-delivery probability had a calculated value of one. After tracing travel paths from every DEM cell, the P_{DEL} values were obtained by subtracting the P_{NO_DEL} grid from one. The resulting grid gave the probability, for every cell in the DEM, of debris-flow delivery from any upslope source point. Probabilities for channel reaches were based on the average value for cells contained in the reach.

3. Description and calibration data for study sites in the Oregon Coast Range

The Oregon Coast Range provides all the conditions for generation of abundant debris flows. Situated on the west coast of Oregon (Fig. 2), it presents sufficient relief (0 to 1200 m) to drive a substantial orographic gradient

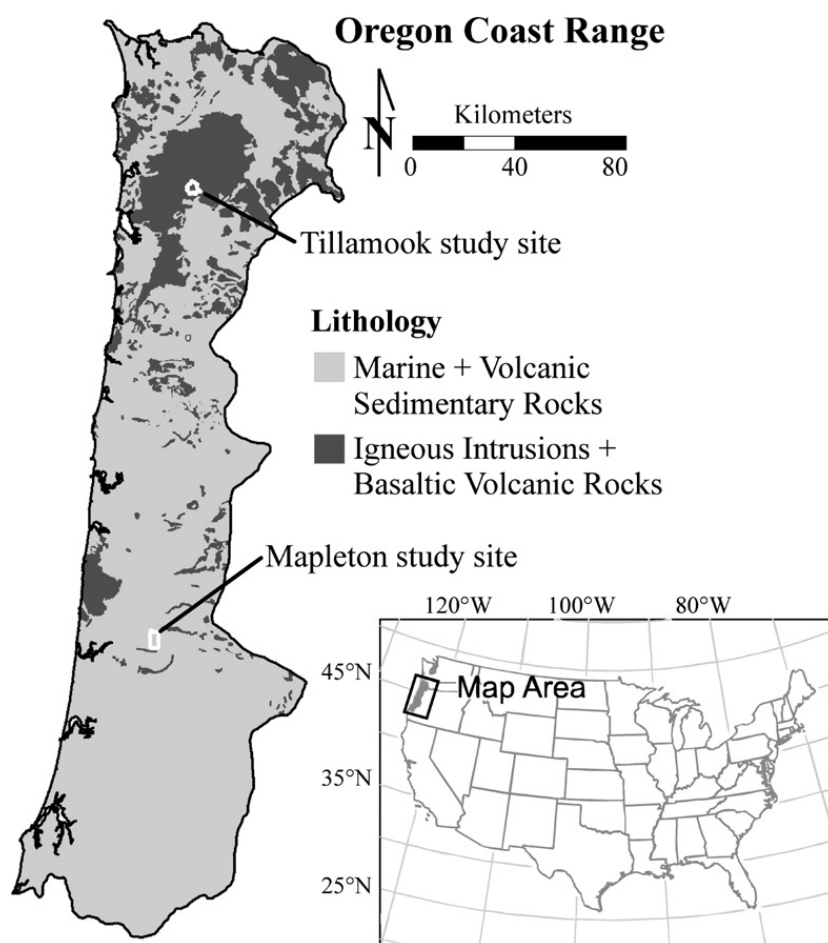


Fig. 2. Location of the field sites for the Oregon Department of Forestry (ODF) debris-flow study in the Oregon Coast Range.

for moisture-laden air moving inland off the Pacific Ocean. Mean-annual precipitation, falling mainly as winter rain, ranges from lows of 1000 mm east of the crest to 5000 mm west of the crest, and includes infrequent, long-duration storms with periods of high intensity (Taylor and Hannan, 1999). Bedrock consists primarily of marine sandstones and shales, with interspersed basaltic volcanics that increase in predominance to the north (Walker and MacLeod, 1991), and maintains steep slopes drained by abundant headwater streams. Slopes are mantled with thin soils that support extensive conifer and hardwood forests, subject in the past to infrequent, severe wildfires, and in modern times to extensive timber harvest and fire suppression (Franklin and Dyness, 1988). These soils are subject to rainfall-triggered landslides, many of which evolve into debris flows that then traverse the steep, headwater channels. In the Coast Range, debris flows form a primary mechanism for bedrock erosion (Stock and Dietrich, 2006) and transfer of sediment from hillslopes to valley floors (Benda, 1990; May and Gresswell, 2004).

Over four days in February 1996, following a wet winter with high antecedent moisture, a high-intensity, long-duration rainstorm caused extensive flooding and triggered thousands of debris flows throughout western Oregon (Hofmeister, 2000). Precipitation totals over the duration of the storm were highly variable and set new records for 4-day total precipitation at some sites (Taylor, 1997).

The Oregon Department of Forestry (ODF) undertook an extensive field-mapping effort, starting in the summer of 1996, to determine landslide frequency and channel impacts (Robison et al., 1999). Three study sites with extensive landsliding were delineated for detailed field mapping. Two of these were in the Oregon Coast Range (Mapleton and Tillamook, Fig. 2) and one (Vida) further east in the Oregon Cascade Range. We calibrated the model for use in the Coast Range, and therefore used data only from Coast Range sites, that from Mapleton for model calibration and evaluation and from Tillamook for model evaluation. The Mapleton site, which encompassed 21.5 km², is entirely underlain by marine sandstones (Fig. 2). Elevations range from 35 m to 660 m with a mean gradient of 0.50. Channel density is 3.1 km km⁻²; the mean channel gradient, including all channels, is 0.19; and (excluding the Siuslaw River, a 7th-order channel of 900 km²) the site includes channels up to 4th order draining up to 12 km². The estimated mean-annual precipitation at the site is 1890 mm (Water and Climate Center of the Natural Resources Conservation Service, 1998). The estimated total precipitation for

the February 1996 storm at the Mapleton site was around 260 mm (Taylor, 1997). In contrast, the Tillamook site, which encompassed 11.7 km², is underlain by basalts (Fig. 2). Elevations range from 211 to 1125 m with a mean gradient of 0.60. Channel density is 6.1 km km⁻²; the mean channel gradient is 0.42; and the site includes channels up to 6th order draining up to 31 km². Estimated mean-annual precipitation is 4000 mm, and estimated total February

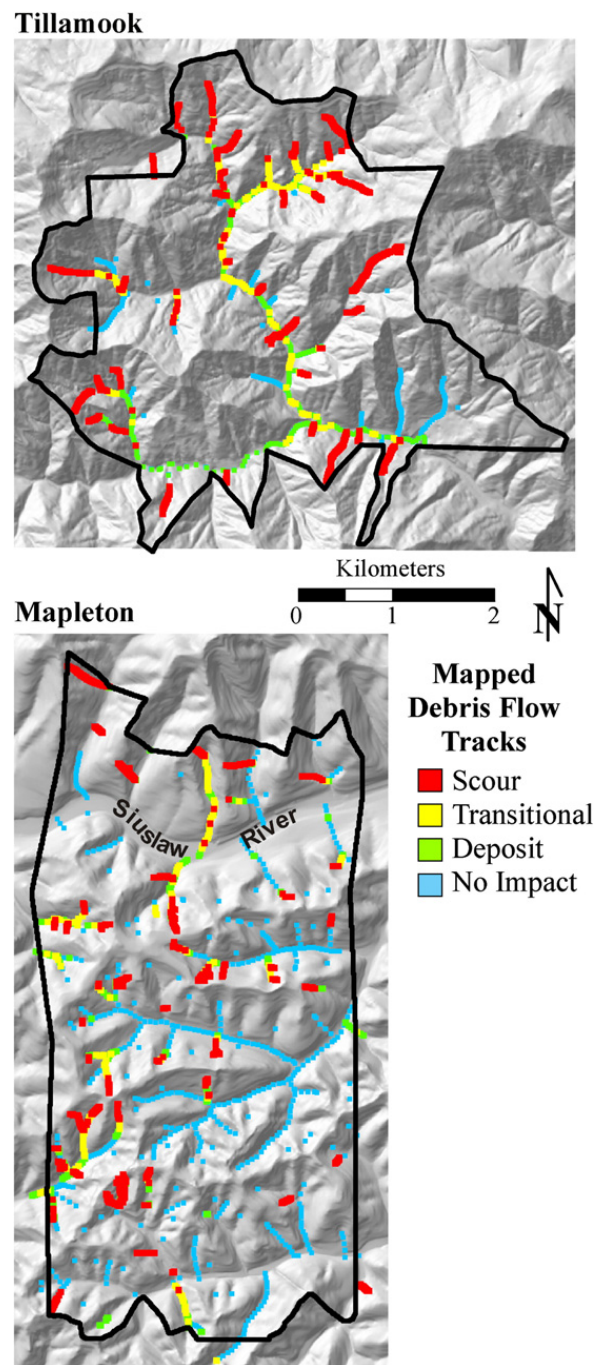


Fig. 3. Map of debris-flow impacts surveyed by the ODF for the Mapleton and Tillamook study sites.

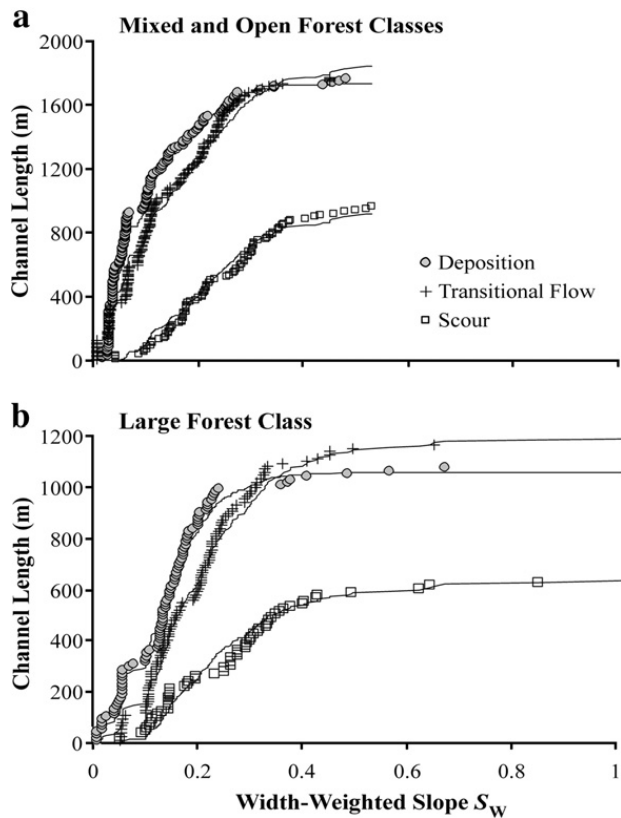


Fig. 4. Cumulative channel length mapped at the Mapleton study site as scour, transitional flow, and deposition plotted against the width-weighted slope, S_W in Eq. (1), for a) Mixed and Open forest classes, and b) Large forest class. Solid lines show the best-fit cumulative distributions. Note the change in vertical scale between the two graphs.

1996 storm precipitation was around 600 mm. At both sites, our analyses included the entire drainage area to every channel, subsequently clipped to the ODF study-site boundaries.

Objectives of ODF's field mapping at these sites were to: find and measure every landslide that delivered sediment to the stream channel; document and measure the associated debris flows and channel impacts; and gather site information regarding forest practices that may have contributed to the impacts (Robison et al., 1999). This storm and ODF's consequent field mapping provided an unprecedented debris-flow data set for the Oregon Coast Range.

Landslide locations and runout tracks to stream channels were mapped by ODF at the Mapleton and Tillamook study sites (Fig. 3). Channel impacts were mapped at 150-foot intervals over the entire channel network, up to channel gradients of 40%. Impacts were classified as none, low, medium, and high. High channel impacts were associated with dam-break floods and debris torrents. Debris-torrent deposits included those from both debris flows and sediment- and debris-laden

fluvial flows. Mapped landslide tracks and channel impacts were divided into zones of scour, transitional flow, and deposition (Robison et al., 1999). We used the mapped landslide locations, runout tracks to the channels, and channels mapped as impacted by debris torrents to estimate debris-flow track locations.

Forest stands were mapped into four age classes (< 10 years, 10–30 years, 31–100 years, > 100 years) by ODF based on harvest history and stand-age mapping provided by landowners and verified using 1:6000-scale aerial photographs taken in the spring and summer of 1996 (Robison et al., 1999). We correlated forest-age class in the study sites with forest cover that was mapped for the entire Oregon Coast Range by Ohmann and Gregory (2002) from Landsat Thematic Mapper imagery (25-m grids) and field plots. From this we delineated three broad forest-cover types: 1) Open (< 10 years): unforested and recently clear-cut harvested, remnant forest, or very-small-diameter (< 10 cm diameter at breast height (dbh)) conifer and hardwood/conifer forest; 2) Mixed (10–100 years): hardwood forest, small- and medium diameter (10–50 cm dbh)

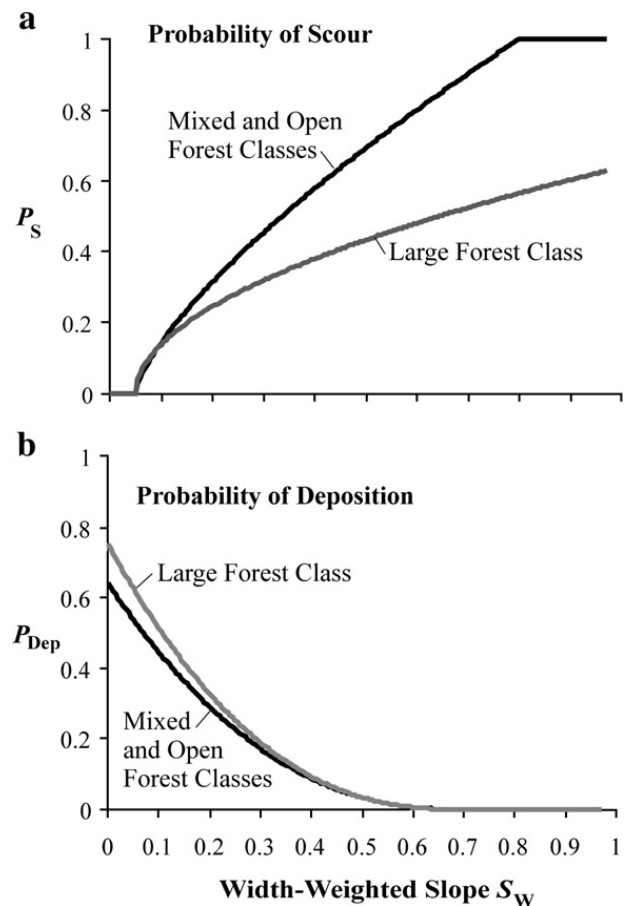


Fig. 5. Probabilities for a) debris-flow scour and b) deposition obtained from least-squares fits to the cumulative distributions in Fig. 4.

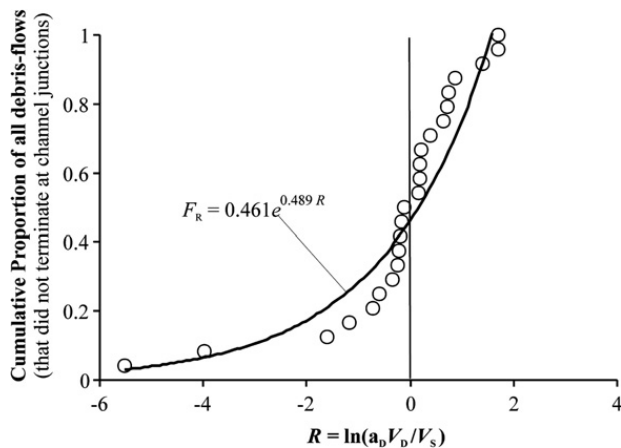


Fig. 6. Cumulative distribution of R values from Eq. (13) for mapped endpoints of the 24 debris flows that did not terminate at channel junctions. Derivative of the fitted curve gives p_R (Eq. (16)), which adjusts the probability that a debris flow terminated within any increment of travel.

conifer and hardwood/conifer forest; and 3) Large (> 100 years): large- and very-large-diameter (> 50 cm dbh) conifer and hardwood/conifer forests. Calibration of probabilities for scour, transitional flow, and deposition were performed separately for each of these three cover types.

DEMs were interpolated over a 10-m grid, with drainage enforcement, from contour lines on USGS 1:24,000-scale topographic maps as described by Clarke and Burnett (2003). Channel networks were delineated using flow paths inferred from the DEMs, as described in Miller (2003). Channel initiation criteria were set to provide the greatest channel density without “feathering” of channels onto unchanneled hillslopes (Montgomery and Foufoula-Georgiou, 1993). The 10-m DEMs provide sufficient topographic detail to resolve greater channel density than indicated by the USGS blue-line channels and identify most of the steep channels subject to debris-flow scour and deposition in the Oregon Coast Range.

4. Results

4.1. Calibration

Mapping by ODF (Robison et al., 1999) from the Mapleton study site (Fig. 3) included 46 separate debris-flow tracks that could be matched, within 30 m, to flow paths determined on the 10-m DEMs. The mapped debris-flow tracks were then overlain on the 25-m-grid forest-cover data and divided between the three cover classes. Tracks that crossed forest-class boundaries were split and divided between the different classes. For each

cover class, weighted-slope values (S_w , Eq. (1)) were calculated for each DEM cell along these tracks and divided between the field-delineated zones of scour, transitional flow, and deposition. Observed and predicted debris-flow-track lengths for these zones are plotted against S_w as cumulative distributions in Fig. 4. Cumulative lengths of scour, transitional flow, and depositional zones were predicted by multiplying the flow length through each DEM cell by the P_S , P_{Dep} , and P_T values obtained for the cell from Eqs. (6)–(8), and then summing over all cells traversed by mapped debris-flow tracks. The five adjustable coefficients in Eqs. (6) and (7) were varied to minimize the squared differences between the observed and predicted cumulative distributions. The resulting P_S and P_{Dep} curves from Eqs. (6) and (7) are shown in Fig. 5. Results for P_S and P_{Dep} in the Open and Mixed forest-cover classes were indistinguishable, but differed from those in the Large forest-cover class (Fig. 5a). In particular, we found that debris flows through older forests had a lower potential for scour.

The next step was to determine a value for the travel-length weighting term, p_R of Eq. (16). Using the functional forms for P_S and P_{Dep} shown in Fig. 5, values for V_S , Eq. (11), and V_D , Eq. (12), were calculated for all cells along the debris-flow tracks. For debris flows from multiple sources that merged into a single track, V_S and V_D were calculated for the single longest track. For the 24 debris flows that did not stop at channel junctions, the median a_D value, Eq. (13), was 0.25, giving the cumulative distribution of R values, Eq. (15), for mapped debris-flow end points shown in Fig. 6. To obtain a weighting value, p_R , as a function of R , the

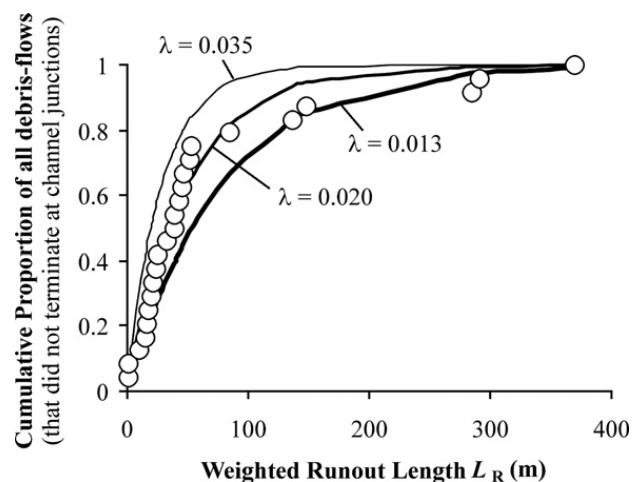


Fig. 7. Cumulative distribution of weighted travel lengths for the 24 debris flows that did not terminate at channel junctions. Solid lines show exponential fits (Eq. (18)) to these points for three values of λ (the rate parameter in an exponential distribution).

cumulative distribution of endpoint R values was fit with an exponential function, with the least-squares fit giving $F_R = 0.461e^{0.489R}$, the derivative of which gives $p_R = 0.226e^{0.489R}$.

Using this form for p_R , weighted travel lengths, L_R of Eq. (17), were calculated for the 24 debris flows (Fig. 7). The mean value, 75.8 m, indicates a probability (or rate) of terminating of 0.013 m^{-1} of weighted travel length. However, a value of 0.02 m^{-1} better represents the distribution of debris flows with weighted travel lengths less than 100 m (Fig. 7); the long-runout debris flows do not fit this model well.

Channel-junction angles (θ_J), debris-flow-volume indices (V_{DF}), and depositional probabilities (P_{Dep}) of the receiving mainstem channel were calculated for all channel junctions intersected by the mapped debris flows (Fig. 8). Based on the calculated values of V_{DF} (Fig. 8), a 20-node serendipity brick was defined that extended from V_{DF} values of -300 to 100 . By definition, P_{Dep} values extend from zero to one and θ_J from 0 to 90° . Every junction traversed by a debris flow and every junction where a debris flow terminated provided a point in the data space. We identified 19 traversed

junctions (“go” junctions) and 22 junctions where debris flows terminated (“stop” junctions). Point densities were calculated over the three-dimensional grid with 60 increments in each dimension, over a radius spanning 20 increments in each dimension. The variation in p_J , the probability that a debris flow traverses a junction, obtained from the resulting interpolation is illustrated over several planes intersecting the data space in Fig. 8. This completes calibration of the debris-flow model.

4.2. Evaluation

Using the procedure described for GIS creation of a P_{DEL} grid, probabilities for debris-flow delivery were calculated for every DEM cell and are shown for channels at the Mapleton and Tillamook study sites in Fig. 9. These probabilities account for the spatial distribution of potential debris-flow sources and intervening topography relative to the channels, and integrate these factors into a single measure of relative potential for debris-flow delivery. These probabilities are based, however, on a relatively small sample size,

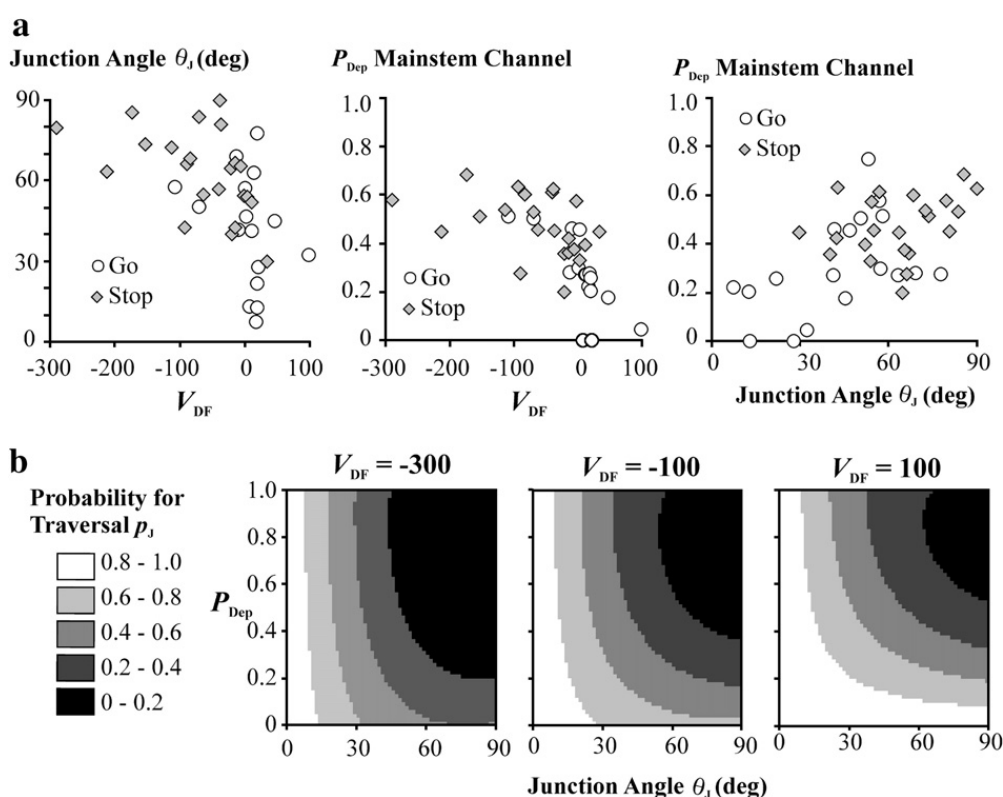


Fig. 8. Observed parameter values at channel junctions and estimated probabilities that a debris flow continues through a junction. a) Scatter plots of observed parameter values for channel junctions intersected by mapped debris flows. P_{Dep} is the probability of debris-flow deposition, Eqs. (5) and (7); and V_{DF} is an index of remaining debris-flow volume, Eq. (20). b) Contours of the estimated probability (p_J) that a debris flow continues through a junction at three values of V_{DF} from cross sections through the 20-node serendipity brick obtained from point densities indicated in Fig. 8a.

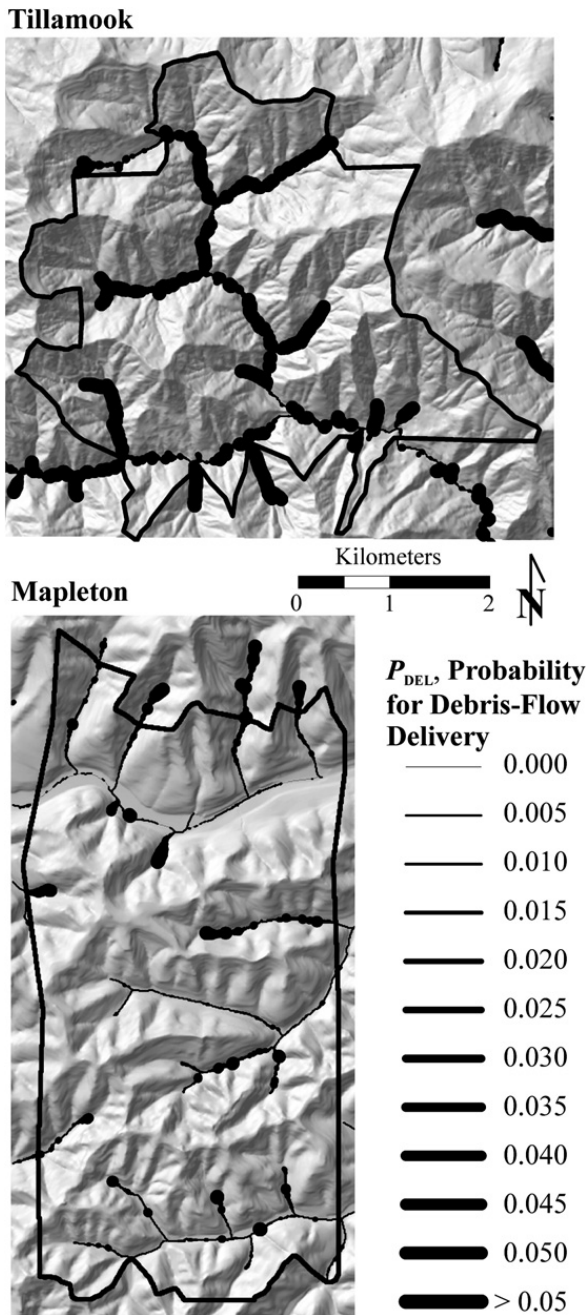


Fig. 9. Calculated probability of finding mapped debris-flows for potentially fish-bearing channels at the Mapleton and Tillamook study sites. Fish-bearing channels are estimated as those with no downstream gradients exceeding 20% and estimated mean-annual flows exceeding $0.01 \text{ m}^3 \text{ s}^{-1}$.

given the range in possible combinations of hillslope topography and channel geometry to be found in a drainage basin.

To assess model output, we compared the distribution of debris-flow locations predicted over the entire study area to those documented by field mapping. Similarity in the predicted and observed distributions suggests that our calibration data are representative of

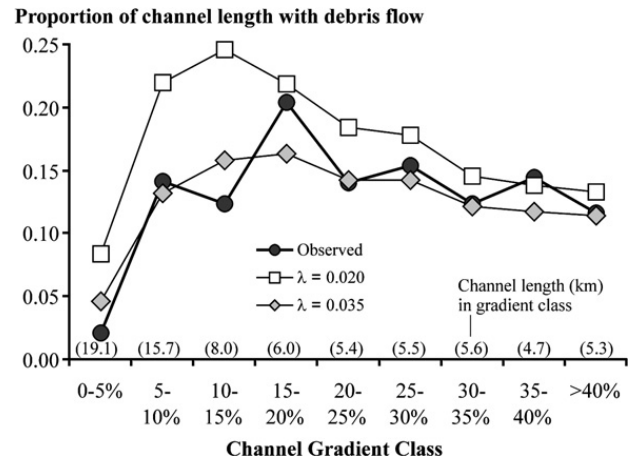


Fig. 10. Predicted and observed proportions of total channel length within the Mapleton study site, divided by gradient class, traversed by debris flows. Predictions were made with two values of λ (rate parameter for the exponential distribution of debris-flow travel lengths, Eq. (18)), for which a λ value of 0.035 best matches the observations.

conditions in the study area and that our model adequately characterizes controls on debris-flow runout. Conversely, dissimilarity in the predicted and observed distributions suggests either that our debris-flow sample was not indicative of those that could occur in the area, or that our model is inadequate.

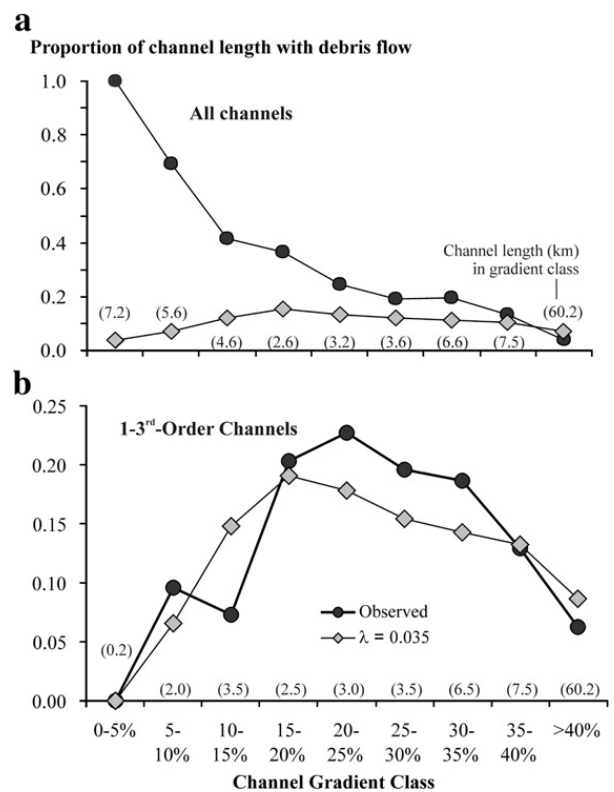


Fig. 11. The proportion of channel length over the Tillamook study site, by gradient class, with mapped and predicted debris-flow impacts, for a) all channels and b) only 1st- through 3rd-order channels.

Our predictions, however, are in terms of probability, not travel length. To translate probability to a prediction of travel length that we could compare directly to field observations, we considered probability in terms of the

proportion of channel segments traversed by debris flows. For example, from a collection of 1000 channel segments chosen from our data set, if each has a calculated probability of 0.01, it is most likely that we

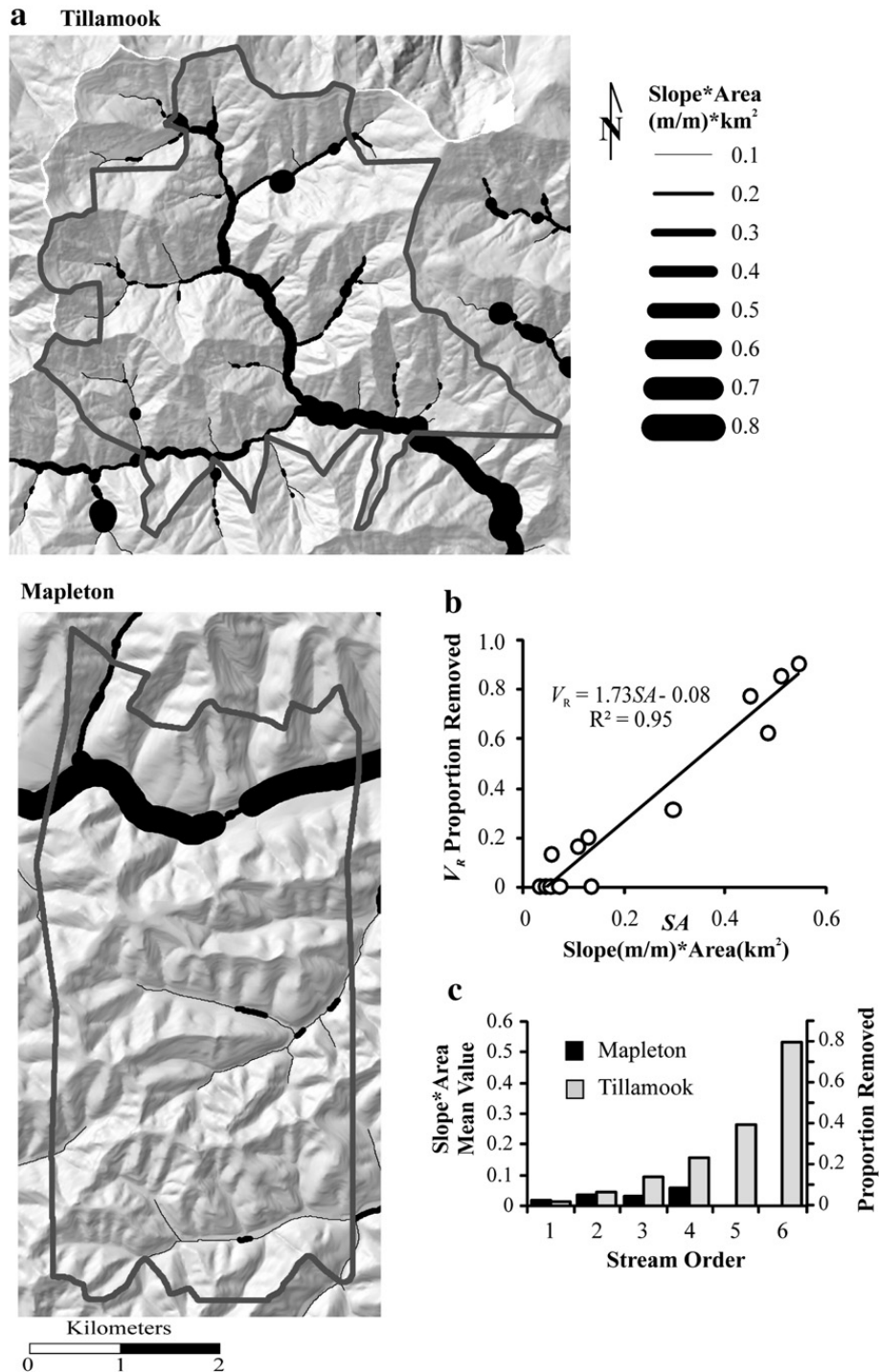


Fig. 12. The effect of slope–area product, an index of total stream power and fluvial transport potential, on the volume of debris-flow deposits remaining in the channel. a) The slope–area product for the Tillamook and Mapleton study sites. b) The proportion of debris-flow-deposit volume remaining in the receiving channel (from Benda, 1990) for deposits < 5 years old as a function of slope–area product. The missing volume was carried downstream by fluvial transport, much of which occurs at the time of deposition. c) Histogram of the mean slope–area product by stream order for the study sites. The right vertical axis shows the proportion of deposit volume removed by fluvial transport based on the linear regression to the data in (b).

will find 10 were traversed by a debris flow. Using this logic, the cumulative length (L_C) traversed by debris flows predicted for any set of channels is

$$L_C = \sum P_{\text{DEL}i} l_i, \quad (25)$$

from which the proportion of those channels traversed by debris flows is given by $L_C / \sum l_i$. Here $P_{\text{DEL}i}$, Eq. (22), is the probability for a debris-flow to travel to the channel traversing the i -th cell, l_i is length of the channel through the i -th cell, and the sum is over all channels specified. For any set of channels, we can then calculate the proportion of channel length traversed by debris flows and compare this prediction with the proportion observed. We assume that the spatial pattern of debris-flow susceptibility indicated by the calibration data is representative of the pattern that would be observed following similar large storms. We do not expect debris flows in exactly the same locations, but we do expect that the terrain attributes associated with debris flows mapped in this study are indicative of channels that have been or will be traversed by debris flows during previous and future storms.

To compare predictions to observed values, we calculated L_C for all delineated channels in the Mapleton study site, divided channels into gradient classes, and compared the proportion of channel length in each class predicted to have been traversed by a debris flow to the proportion with mapped debris flows (Fig. 10). Using the parameter values from the calibration described previously, we found that L_C tended to over-predict the proportion of low-gradient channel length with debris flows, relative to the results from the calibration data set (Fig. 10). Over-prediction of travel length in low-gradient channels suggests that we under-estimated the value of λ , the probability of terminating per unit length of travel, since low-gradient channels tend to occur at the downstream end of debris-flow runout tracks. Calculated L_C values matched observations more closely when λ was increased from 0.02 to 0.035 (Fig. 10). We could choose a value to match either the empirical distribution of individual weighted travel lengths (Eq. (18) and Fig. 7), or the empirical distribution of travel lengths over different stream gradients (Eq. (25) summed over all channels in a gradient class, and Fig. 10). We chose the latter, because we are ultimately interested in characterizing debris-flow effects on low-gradient, fish-bearing streams, not in predicting runout lengths for individual debris flows. This added one more step to our calibration procedure and indicated an inability of this model to effectively represent both the distribution of individual debris-flow

travel lengths and the distribution of channel gradients affected by the debris flows represented in this data set. By adding this last calibration step, we emphasized the distribution of stream gradients sampled by these debris flows at the expense of the predicted distribution of total lengths.

The ODF mapping from the Tillamook study area provides a separate data set to compare with model predictions. Field mapping there (Robison et al., 1999) indicated that all channels with gradients less than 5% (2.9°) contained evidence of debris-torrent passage (Figs. 3 and 11a), whereas model predictions indicate that only about 4% of these channels would be traversed by debris flows (Fig. 11a). This discrepancy may reflect differences in the nature of the mainstem channels between the Mapleton and Tillamook sites. Effects of debris-flow deposition in mainstem channels depend on the potential for fluvial transport of material forming the deposit. Channels are typically steeper at the Tillamook than at the Mapleton site, and, except for the Siuslaw River in the Mapleton site, the Tillamook site includes larger channels (Fig. 12). Benda et al. (2003) found that small debris flows, under 1000 m³, depositing into relatively large or steep rivers, with a slope–area product greater than about 0.3 km², tended to have a large proportion of their volume carried downstream by the receiving channel. In these cases, debris-flow material can contribute to fluvial deposits for long distances downstream (e.g., Miller and Benda, 2000).

To estimate the potential for downstream fluvial transport of debris-flow material, we used data presented by Benda (1990, Fig. 3 on pp. 461) that relate the proportion of debris-flow-deposit volume remaining to drainage area of the receiving channel. For deposits 5 years or less in age, Benda (1990) estimated total deposit volume from the geometry and length of scoured zones along the associated debris-flow tracks, and determined volume remaining from ground surveys. We plotted Benda's (1990) results for the proportion of volume remaining against the slope–area product (Fig. 12b), rather than drainage area alone, using data for each site from Benda (1988). Although a bit sparse in the midrange, the data clearly show that erosion of debris-flow deposits was greater in larger and steeper channels. A linear regression through the points gives V_R , the proportion of volume removed, as a function of slope–area product SA:

$$V_R = 1.73SA - 1.08. \quad (26)$$

Average debris-flow volumes at both the Tillamook and Mapleton study sites, determined from the estimated

volume of material eroded along the scoured portion of the runout track, were relatively small, under 1000 m^3 (Robison et al., 1999). However, slope–area products for third- and higher-order channels were considerably higher at Tillamook than at Mapleton (Fig. 12c), leading, we suspect, to different consequences in the mainstem channels. From Eq. (26), we estimated the proportion of debris-flow deposits potentially carried downstream by fluvial transport during the flood associated with the 1996 storm (Fig. 12c). The small proportions predicted for the Mapleton site suggests that debris flows there formed distinct deposits within mainstem valleys, whereas the larger proportions predicted for the Tillamook site suggests that debris

flows there had much of their volume carried downstream, triggering the extensive downstream channel disturbance mapped by ODF. If we look solely at third- and lower-order channels, the debris-flow model predicts the extent of channel length impacted by debris flows for Tillamook quite well (Fig. 11b).

5. Discussion

5.1. Applications

This model was developed to examine the role of debris-flows in Oregon Coast Range stream ecosystems. Because it was built on and calibrated with 1:24,000-

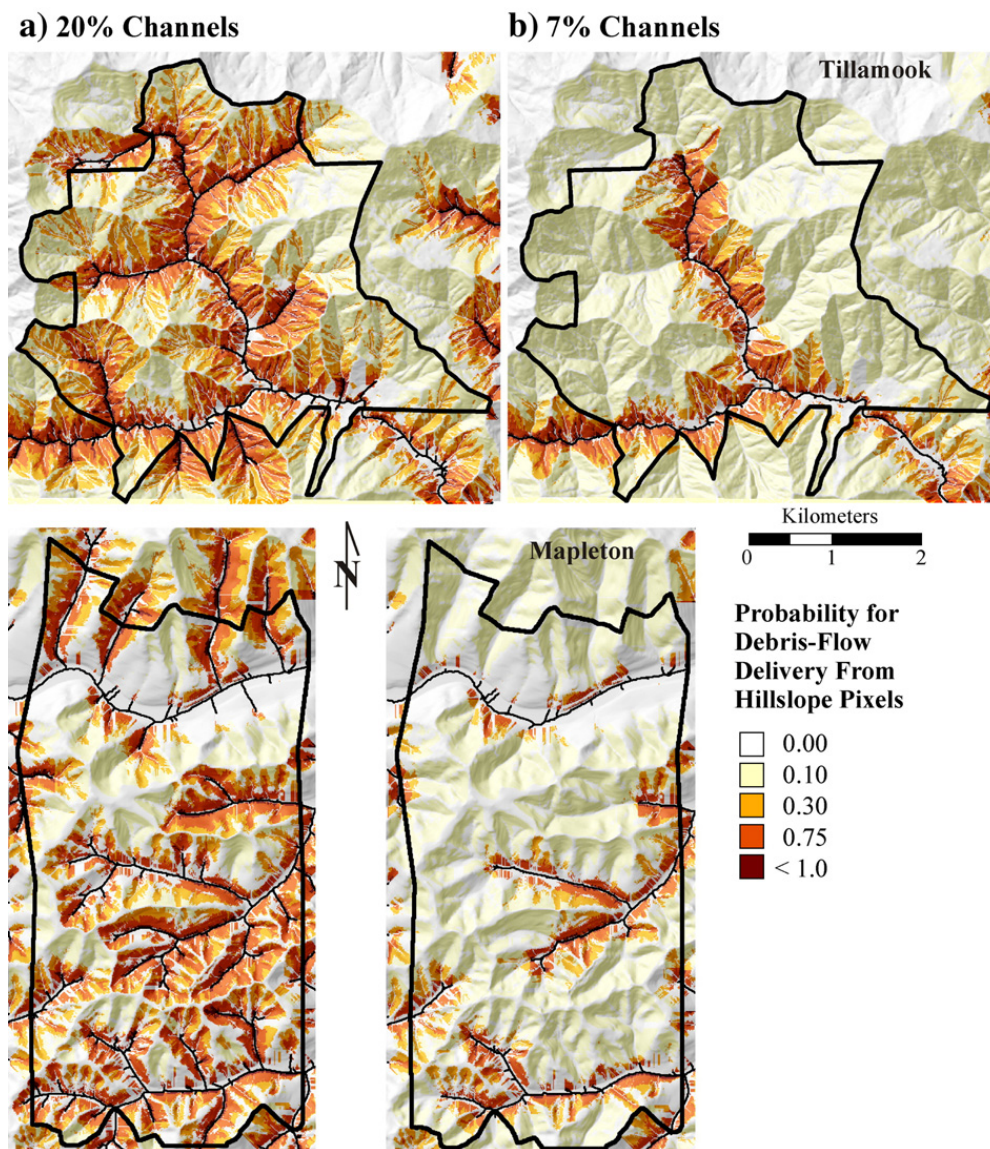


Fig. 13. The calculated probability for a debris flow to travel from each hillslope DEM cell to channels with a) downstream gradients $\leq 20\%$, representing all potentially fish-bearing streams, and b) downstream gradients $\leq 7\%$, representing all potentially coho-bearing streams, for the Tillamook and Mapleton study sites.

scale topographic data (10-m DEMs), it predicts the probability for debris-flow delivery to streams over reach scales of 10^1 to 10^2 m (Fig. 9). This resolution highlights along-channel variability in debris-flow potential, which allows direct comparison of model predictions to surveys of channel geomorphology and aquatic habitat. For example, we expect reaches with a high debris-flow probability to have a high probability of exhibiting evidence of past debris-flow deposition (fans, terraces, boulders, and large wood). Ultimately, predictions of debris-flow susceptibility should improve predictions of habitat types, disturbance regimes, and the associated distribution of species assemblages, abundance, and productivity over entire channel networks (e.g., Burnett et al., 2007).

The model also provides a direct process linkage between hillslopes and stream channels. It identifies debris-flow source areas and links them to the specific channel reaches affected. The probability for debris-flow delivery from a single source point to a specific channel location can be mapped over all sources. For instance, the model indicates distinct differences in the distribution of hillslope locations from which debris flows can reach the fish-bearing portion of a channel network and the portion of the network accessible to coho salmon (*Oncorhynchus kisutch*) (Fig. 13). Model predictions are being developed and tested as tools for

highlighting potential debris-flow producing zones for use in timber-harvest planning and for stream restoration and conservation efforts (Benda et al., 2007; Burnett and Miller, 2007).

The model can be applied and the results integrated over a range of spatial extents. By calculating the cumulative debris-flow travel length, L_C in Eq. (25), over identified channels (excluding unchannelized hillslopes), the spatial density (length per unit area) of debris-flow-affected channels can be estimated over any basin scale (Fig. 14). This allows basins to be ranked in terms of potential debris-flow impacts that quantify the variable effects of regional and local topography.

5.2. Effect of forest cover on debris-flow scour and runout length

In general, the proportion of channel length mapped by ODF as scoured at the Mapleton site was greater in the Open and Mixed classes than in the Large class, so that our calibration for probability of scour differed between the Large class and the other two forest classes (Fig. 5a). Such differences in the degree of debris-flow scour between forest types have been observed elsewhere. Field surveys from the western Olympic mountains Washington, USA indicated that “Debris flows in the industrial forest leave channels scoured to

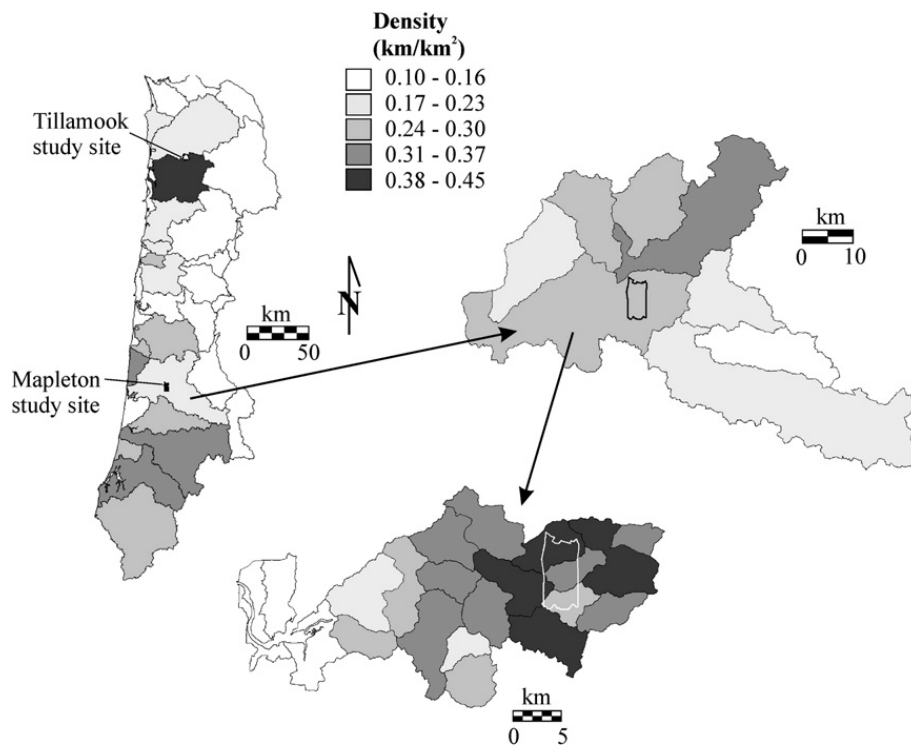


Fig. 14. The calculated density of debris-flow impacted channels over three spatial scales. Spatial scales correspond to 5th-, 6th-, and 7th-field USGS Hydrologic Units.

bedrock along much of their length, but in the old growth such scour is rare, and reaches tend to retain sediment cover along most of their length” (Bunn and Montgomery, 2000, pp. 106). Industrial forests correspond to our Open and Mixed forest-cover classes, old growth to our Large class. In field surveys in southeast Alaska, clearcuts tended to have greater erosion volumes per unit length of debris-flow travel than did old-growth forests (Johnson et al., 2000) for slope classes greater than 16% (9°), with deposition occurring in both forest types for slope classes less than 16%.

The lower potential for debris-flow scour in the Large forest class (Fig. 5a) results in shorter estimates of scour length and smaller entrained volumes (Eq. (11)) along debris-flow tracks through this class than through the Open and Mixed classes. Smaller entrained volumes lead to shorter predicted runout lengths; hence, the model predicts lower probabilities for runout through mature forests than through clearcuts and young forest stands. For example, if we keep all the landslide initiation probabilities as originally estimated, but calculate runout probabilities first for uniformly unfor-ested conditions (Open class) and then for uniformly forested conditions (Large class), we predict that the cumulative length of channels traversed by debris flows will be reduced by 20% (from 8256 m to 6600 m, Eq. (25)) for the Mapleton study area. This reduction is solely a consequence of the difference in the calibrated probability for debris-flow scour found between the Open and Large forest-cover classes (Fig. 5a).

Our prediction of shorter debris-flow runout lengths through older forests is consistent with empirical findings. In analyzing the ODF data, which included data for the Mapleton study site, Robison et al. (1999) also noted differences in runout lengths for debris flows in different forest-age classes. They used threshold values of channel gradient and channel-junction angles, as described by Benda and Cundy (1990), to determine expected debris-flow lengths. Debris flows that did not go as far as expected traveled predominately through mature forests (Robison et al., 1999). May (2002) also surveyed debris flows in coastal Oregon following the 1996 storm. Although surveyed values varied greatly, May (2002) found the lowest mean runout length for debris flows through mature forests.

Although our model suggests that differences in runout length between forest classes may result from differences in the extent of scour zones, other mechanisms must also influence travel length. For example, May (2002) found that volumes eroded per unit length of debris-flow travel through scour zones tended to be greater in mature forests than in clearcuts or second-

growth forests, which would counter the effect of shorter scour lengths in mature forests. Other factors affecting runout length include suppression of debris-flow travel through depositional zones in forested areas, relative to unfor-ested areas, as reported by Ishikawa et al. (2003) for sites in Japan. Additionally, Lancaster et al. (2003) demonstrated with a mechanistic model that entrainment and transport of wood should suppress debris-flow movement. Differences among forest classes in abundance of large standing and down trees in and along stream channels may then also affect runout lengths.

5.3. Limitations

Model calibration and resulting empirical probabilities reference mapping from a single storm event. Because this was a large-magnitude storm that triggered many debris flows, we expect that the mapped debris-flow tracks well represent intrinsic controls on debris-flow runout. However, this assumption waits testing against data collected over longer time periods that include a greater range of storm characteristics and antecedent conditions.

Likewise, modeled probabilities of debris-flow delivery reflect the number of events mapped following a single storm at a single study site; they do not reflect rates of occurrence or probabilities over time. This is an important distinction. We use model results only as indicators of relative rates. Calibration to estimate actual rates requires time-series data (e.g., Reid and Page, 2002).

The model is intended for medium and regional scale analyses ($\sim 1:24,000$ scale, Soeters and van Westen, 1996). The resolution of underlying data and the assumptions inherent in model design preclude its use for site-scale analyses of debris-flow hazards. It can be used to identify areas prone to debris-flow occurrence, but determination of the need for and design of specific mitigation measures requires more detailed aerial photograph and field-based observations.

The model, as currently set up, requires estimates of 29 parameters (Table 2). All parameter values are calibrated to field observations. In fact, all parameters, except for a_D and λ , are used simply to provide a smooth interpolating function to field-measured proportions. We could use the measured proportions directly, but the functional forms are more easily implemented in an automatic scheme for computing their values.

Nevertheless, 29 parameters provide great leeway for model adjustment. Calibration builds progressively from estimates of where scour and deposition occur to the probability that a debris flow terminates. Parameters

Table 2
Model parameter values

W_{V1}	12 m	Mean confining width of 1st-order channels, Eq. (2)
S_{W1} (scour) Open forest class	0.8	S_W value above which only debris-flow scour occurs, Eqs. (9) and (10)
S_{W1} (scour) Large forest class	2.3	
S_{W0} (deposit) Open forest class	-0.15	S_W value below which only deposition occurs; least-squares fit gives negative value, Eqs. (9) and (10)
S_{W0} (deposit) Large forest class	-0.09	
S_{W1} (deposit) Open forest class	0.7	S_W value above which no deposition occurs, Eqs. (9) and (10)
S_{W1} (deposit) Large forest class	0.7	
c_S Open forest class	0.72	Scour exponent for Eq. (6)
c_S Large forest class	0.52	
c_{Dep} Open forest class	2.34	Deposit exponent for Eq. (7)
a_D	0.25	Proportionality constant between V_D and V_S , Eq. (13)
a , where $p_R = a * \exp^{bR}$	0.226	From exponential fit to distribution of debris-flow endpoint R values, Fig. 5
b , where $p_R = a * \exp^{bR}$	0.489	
λ	0.035	“Rate” parameter for exponential distribution of debris-flow travel lengths, Eqs. (18) and (19)
P1	0.000	Serendipity-brick point values, Fig. 2
P2	0.000	
P3	0.015	
P4	0.691	
P5	0.000	
P6	0.000	
P7	0.778	
P8	1.000	
P9	0.000	
P10	0.007	
P11	0.560	
P12	0.650	
P13	0.000	
P14	0.000	
P15	0.668	
P16	0.903	
P17	0.000	
P18	0.658	
P19	0.845	
P20	0.803	

calibrated late in the sequence can compensate for uncertainties in parameters calibrated early in the sequence. For example, changes in coefficients for P_S

and P_{Dep} in Eqs. (6) and (7), and for a_D in Eq. (13), alter the calibrated values for parameters in later steps. The last step, choice of a value for λ , the probability that a debris flow terminates per unit length of travel, thus has a large influence on model results. We only needed to adjust λ to better fit the observed distribution of debris-flow-affected channel length by gradient (Fig. 10). However, by focusing our evaluation only on channel gradient, we miss other types of spatial variation that may be more sensitive to changes in P_S and P_{Dep} . We used channel gradient because it is a key factor influencing where fish are found in a stream network, but other concerns (e.g., effects of standing trees on debris-flow runout length) would direct our attention elsewhere. We endeavored to build a model based on rational relationships between available debris-flow mapping, available digital data, and logical physical constraints. However, the value of an empirical model, particularly one with so many parameters, is proven only by its ability to reproduce observations in areas beyond the calibration area. The match to mapping in first- through third-order channels at the Tillamook study site is reassuring, but our inability to predict downstream impacts at Tillamook highlights a current shortcoming of this model.

Assumptions made to develop this model point to ways of improving it. Estimates of volume entrained, V_S of Eq. (11), assume that the volumes available for entrainment per unit scour length are derived from a spatially uniform distribution, but this is not the case. The volume available for scour from any potential debris-flow track is largely a function of the time since the last debris flow (May and Gresswell, 2003) and varies from site to site (May, 2002). If the probability of debris-flow delivery, P_{DEL} of Eq. (22), is proportional to the frequency of debris-flow events through steep, low-order channels, then the volume accumulated should, on average, be proportional to the inverse of P_{DEL} . Likewise, systematic differences in erosion and deposition rates ($m^3 m^{-1}$) through zones of scour and deposition in different forest classes suggest that a_D , the proportionality constant of Eq. (13), should be set independently for each class.

Our estimates of debris-flow volume also lack the volume of the initiating landslide. This is a minor effect if the initiating volume is small relative to the volume entrained during runout, but the initiating volume can comprise a large portion of the resulting debris-flow deposit (May, 2002). A model that includes some estimate of initiating volume may better represent the full range of runout lengths (Fig. 7), particularly if long-runout debris flows tend to have larger than average initiating volumes.

Our estimate of volume deposited, V_D , Eq. (12), ignores the constraints imposed by debris fans at channel junctions. These fans are generally too small to be resolved from 1:24,000-scale topographic data, yet fans can be a primary factor limiting debris-flow delivery of material to larger streams (May and Gresswell, 2004). These effects are partially accounted for in our calibration for p_J , the probability that a debris flow traverses a junction, but a more direct accounting of fan size and geometry may better constrain estimates of this probability. Fan size and geometry vary with the number of debris-flow sources in the contributing basin, the size of the receiving channel, and the time since the last debris flow (May and Gresswell, 2004), all of which could be incorporated into this modeling framework.

We have not evaluated the influence of geology or soil types on debris-flow runout. The model could be calibrated separately for different geologies and soils. Our results (Fig. 11) suggest that the model calibration from Mapleton can be reasonably extrapolated to low-order channels throughout the Oregon Coast Range, but that further strategies are required to assess potential downstream impacts in rock types other than sandstones. Inclusion of attributes that gauge the potential for fluvial transport of debris-flow-delivered material, such as a measure of stream power (Fig. 12), may improve our ability to predict debris-flow impacts in the receiving channels.

6. Conclusions

Available 10-m elevation and 25-m land-cover digital data provide sufficient information to resolve the distribution of debris-flow delivery locations for channels over regional extents. We have presented methods for using these data with field-mapped debris-flow track locations to calculate a relative susceptibility to debris-flow delivery for all channels in a given area. For the calibration area, these methods reproduce, within 5%, the cumulative length of channels with mapped debris flows. When applied to another area with different geology (basaltic rock types versus sandstone at the calibration site), steeper slopes and channels, and higher drainage density, we find that the methods predict cumulative mapped debris-flow length for low-order channels within 5%, but under-predict mapped debris-flow lengths for larger channels. We suspect that these differences are explained by the larger stream power for 4th- and 5th-order channels at the test site than found at the calibration site, but this hypothesis awaits further testing.

We have developed a modeling approach to quantify channel susceptibility to debris-flow inputs that

accounts for hillslope topography, channel-network geometry, and forest cover, using digital data that can be widely applied with a GIS. Because these data leave much variability in controlling factors unquantified, we chose a probabilistic model design. Comparison with widely separated field sites suggests that the model can be robustly extrapolated for low-order channels, but that further strategies are needed to characterize consequences for larger channels. The ability to use available data to quantify debris-flow runout potential opens the door to developing a variety of tools for assessing landslides, channel conditions, and land-management effects on watershed processes.

Acknowledgements

This research was conducted as part of the Coastal Landscape Analysis and Modeling Study (CLAMS). The USDA Forest Service Pacific Northwest Research Station and Earth Systems Institute provided financial support for this work. We thank the Oregon Department of Forestry for the assistance in obtaining and interpreting the survey data from their 1996 storm study. Jim Paul and Jason Hinkle with the ODF were both particularly helpful.

References

- Bathurst, J.C., Burton, A., Ward, T.J., 1997. Debris flow run-out and landslide sediment delivery model tests. *Journal of Hydraulic Engineering* 123, 410–419.
- Benda, L., 1988. Debris flows in the Tyee Sandstone Formation of the Oregon Coast Range, M.S. Thesis, University of Washington, Seattle, WA.
- Benda, L.E., 1990. The influence of debris flows on channels and valley floors in the Oregon Coast Range, U.S.A. *Earth Surface Processes and Landforms* 15, 457–466.
- Benda, L.E., Cundy, T.W., 1990. Predicting deposition of debris flows in mountain channels. *Canadian Geotechnical Journal* 27, 409–417.
- Benda, L.E., Veldhuisen, C., Black, J., 2003. Debris flows as agents of morphological heterogeneity at low-order confluences, Olympic Mountains, Washington. *Geological Society of America Bulletin* 115, 1110–1121.
- Benda, L.E., Poff, L., Miller, D.J., Dunne, T., Reeves, G.H., Pess, G.R., Pollock, M.M., 2004. The network dynamics hypothesis: how channel networks structure riverine habitats. *BioScience* 54, 413–427.
- Benda, L.E., Miller, D.J., Andras, K., Bigelow, P., Reeves, G.H., Michael, D., 2007. NetMap: a new tool in support of watershed science and resource management. *Forest Science* 53, 206–219.
- Bigelow, P.E., Benda, L.E., Miller, D.J., Burnett, K.M., 2007. On debris flows, river networks, and the spatial structure of channel morphology. *Forest Science* 53, 220–238.
- Brummer, C.J., Montgomery, D.R., 2003. Downstream coarsening in headwater channels. *Water Resources Research* 39, 1294. doi:10.1029/2003WR001981.
- Bunn, J.T., Montgomery, D.R., 2000. Patterns of wood and sediment storage along debris-flow impacted headwater channels in old-

- growth and industrial forests of the western Olympic mountains, Washington. In: Bennet, S.J., Simon, A. (Eds.), *Riparian Vegetation and Fluvial Geomorphology*. American Geophysical Union, Washington D.C., pp. 99–112.
- Burnett, K.M., Miller, D.J., 2007. Streamside policies for headwater channels: an example considering debris flows in the Oregon Coastal Province. *Forest Science* 53, 239–253.
- Burnett, K.M., Reeves, G.H., Miller, D.J., Clarke, S., Vance-Borland, K., Christiansen, K., 2007. Distribution of salmon-habitat potential relative to landscape characteristics and implications for conservation. *Ecological Applications* 17, 66–80.
- Cannon, S.H., 1993. An empirical model for the volume-change behavior of debris flows. In: Shen, H.W., Su, S.T., Wen, F. (Eds.), *Proceedings, Hydraulic Engineering '93*. American Society of Civil Engineers, New York, pp. 1768–1777.
- Cenderelli, D.A., Kite, J.S., 1998. Geomorphic effects of large debris flows on channel morphology at North Fork Mountain, Eastern West Virginia, USA. *Earth Surface Processes and Landforms* 23, 1–19.
- Clarke, S., Burnett, K., 2003. Comparison of digital elevation models for aquatic data development. *Photogrammetric Engineering and Remote Sensing* 69, 1367–1375.
- Dietrich, W.E., Dunne, T., 1978. Sediment budget for a small catchment in mountainous terrain. *Zeitschrift für Geomorphologie*. Supplementband 29, 191–206.
- Dunne, T., 1998. Critical data requirements for prediction of erosion and sedimentation in mountain drainage basins. *Journal of the American Water Resources Association* 34, 795–808.
- Ellen, S.D., Mark, R.K., 1993. Mapping debris-flow hazard in Honolulu using a DEM. In: Shen, H.W., Su, S.T., Wen, F. (Eds.), *Proceedings, Hydraulic Engineering '93*. American Society of Civil Engineers, New York, pp. 1774–1779.
- Fannin, R.J., Rollerson, T.P., 1993. Debris flows: some physical characteristics and behavior. *Canadian Geotechnical Journal* 30, 71–81.
- Fannin, R.J., Wise, M.P., 2001. An empirical-statistical model for debris flow travel distance. *Canadian Geotechnical Journal* 38, 982–994.
- Franklin, J.F., Dyrness, C.T., 1988. *Natural Vegetation of Oregon and Washington*. Oregon State University Press, Corvallis, Oregon. 464 pp.
- Hack, J.T., Goodlett, J.C., 1960. *Geomorphology and forest ecology of a mountain region in the central Appalachians*. US Geological Survey Professional Paper, vol. 347. US Geological Survey, Washington, D.C.
- Hofmeister, R.J., 2000. Slope failures in Oregon. GIS Inventory for Three 1996/97 Storm Events. Special Paper 34. Oregon Dep. of Geology and Mineral Industries, Portland.
- Hofmeister, R.J., Miller, D.J., 2003. GIS-based modeling of debris-flow initiation, transport and deposition zones for regional hazard assessments in western, Oregon, USA. In: Reickenmann, D., Chen, C. (Eds.), *Debris-Flow Hazards Mitigation: Mechanics, Prediction, and Assessment*. Millpress, Rotterdam, pp. 1141–1149.
- Ishikawa, Y., Kawakami, S., Morimoto, C., Mizuhara, K., 2003. Suppression of debris movement by forests and damage to forests by debris deposition. *Journal of Forest Research* 8, 37–47.
- Iverson, R.M., 1997. The physics of debris flows. *Reviews of Geophysics* 35, 245–296.
- Iverson, R.M., Schilling, S.P., Vallance, J.W., 1998. Objective delineation of lahar-inundation hazard zones. *Geological Society of America Bulletin* 110, 972–984.
- Johnson, A.C., Swanston, D.N., McGee, K.E., 2000. Landslide initiation, runout, and deposition within clearcuts and old-growth forests of Alaska. *Journal of the American Water Resources Association* 36, 17–30.
- Lancaster, S.T., Hayes, S.K., Grant, G.E., 2003. Effects of wood on debris flow runout in small mountain watersheds. *Water Resources Research* 39, 1168. doi:10.1029/2001WR001227.
- May, C.L., 2002. Debris flows through different forest age classes in the central Oregon Coast Range. *Journal of the American Water Resources Association* 38, 1–17.
- May, C.L., Gresswell, R.E., 2003. Processes and rates of sediment and wood accumulation in headwater streams of the Oregon Coast Range, USA. *Earth Surface Processes and Landforms* 28, 409–424.
- May, C.L., Gresswell, R.E., 2004. Spatial and temporal patterns of debris-flow deposition in the Oregon Coast Range, USA. *Geomorphology* 57, 135–149.
- Miller, D.J., 2003. Programs for DEM analysis, in *Landscape dynamics and forest management*. Gen. Tech. Rep. RMRS-GTR-101CD, USDA Forest Service, Rocky Mountain Research Station, Fort Collins, CD-ROM.
- Miller, D.J., Benda, L.E., 2000. Effects of punctuated sediment supply on valley-floor landforms and sediment transport. *Geological Society of America Bulletin* 112, 1814–1824.
- Miller, D.J., Burnett, K.M., 2007. Effects of forest cover, topography, and sampling extent on the measured density of shallow, translational landslides. *Water Resources Research* 43, W03433. doi:10.1029/2005WR004807.
- Montgomery, D.R., Foufoula-Georgiou, E., 1993. Channel network source representation using digital elevation models. *Water Resources Research* 29, 3925–3934.
- Montgomery, D.R., Schmidt, K.M., Greenberg, H.M., Dietrich, W.E., 2000. Forest clearing and regional landsliding. *Geology* 28, 311–314.
- Ohmann, J.L., Gregory, M.J., 2002. Predictive mapping of forest composition and structure with direct gradient analysis and nearest neighbor imputation in coastal Oregon, USA. *Canadian Journal of Forest Resources* 32, 725–741 <http://www.fsl.orst.edu/clams/>.
- Reid, L.M., Page, M.J., 2002. Magnitude and frequency of landsliding in a large New Zealand catchment. *Geomorphology* 49, 71–88.
- Rickenmann, D., 1999. Empirical relationships for debris flows. *Natural Hazards* 19, 47–77.
- Robison, G.E., Mills, K.A., Paul, J., Dent, L., Skaugset, A., 1999. *Storm Impacts and Landslides of 1996: Final Report*. Oregon Department of Forestry, Salem, OR.
- Schilling, S.P., 1998. LAHARZ: GIS programs for automated mapping of lahar-inundation hazard zones. Open-File Report 98–638. U.S. Geological Survey, Vancouver, WA.
- Soeters, R., van Westen, C.J., 1996. Slope instability recognition, analysis, and zonation. In: Turner, A.K., Schuster, R.L. (Eds.), *Landslides Investigation and Mitigation*, Transportation Research Board Special 247. National Academy Press, Washington, D.C., pp. 129–177.
- Stock, J.D., Dietrich, W.E., 2006. Erosion of steepland valleys by debris flows. *Geological Society of America Bulletin* 118, 1125–1148.
- Swanson, F.J., Dyrness, C.T., 1975. Impact of clearcutting and road construction on soil erosion by landslides in the western Cascade Range, Oregon. *Geology* 3, 393–396.
- Swanson, F.J., Kratz, T.K., Caine, N., Woodmansee, R.G., 1988. Landform effects on ecosystem patterns and processes. *BioScience* 38, 92–98.
- Swanson, F.J., Johnson, S.L., Gregory, S.V., Acker, S.A., 1998. Flood disturbance in a forested mountain landscape. *BioScience* 48, 681–689.

- Taylor, G.H., 1997. The great flood of 1996. Oregon Climate Service. Available at <http://www.ocs.oregonstate.edu>.
- Taylor, G., Hannan, C., 1999. The Climate of Oregon: From Rain Forest to Desert. Oregon State University Press, Corvallis, OR.
- Walker, G.W., MacLeod, N.S., 1991. Oregon Geology, 1:500,000 map scale, 2 sheets, US Department of the Interior, Geological Survey, Reston, VA.
- Water and Climate Center of the Natural Resources Conservation Service, 1998. Oregon Average Monthly or Annual Precipitation, 1961–90. Available at <http://www.ocs.orst.edu/prism/products/>.
- Wohl, E.E., Pearthree, P.P., 1991. Debris flows as geomorphic agents in the Huachuca Mountains of southeastern Arizona. *Geomorphology* 4, 273–292.
- Zevenbergen, L.W., Thorne, C.R., 1987. Quantitative analysis of land surface topography. *Earth Surface Processes and Landforms* 12, 47–56.
- Zienkiewicz, O.C., Taylor, R.L., 1988. *The Finite Element Method*, vol. 1. McGraw-Hill, London.